BULLETIN OF THE POLISH ACADEMY OF SCIENCES
TECHNICAL SCIENCES, Vol. 74(6), 2026, Article number: 6593
DOI: 10.24425/bpasts.2026.6593

Influence of counter-running wave interference on operation of the PT-symmetric structures

Agnieszka MOSSAKOWSKA-WYSZYŃSKA[1]*, **Piotr WITOŃSKI**[1], **Michał RĘKAWEK**[2], and **Paweł SZCZEPAŃSKI**[1,3]

[1] Institute of Microelectronics and Optoelectronics, Warsaw University of Technology, ul. Koszykowa 75, 00-665 Warsaw, Poland
[2] Łukasiewicz Research Network, Institute of Microelectronics and Photonics, Al. Lotników 32/46, 02-668 Warsaw, Poland
[3] National Institute of Telecommunications, ul. Szachowa 1, 04-894 Warsaw, Poland

Abstract. This work provides a theoretical investigation of how counter-propagating wave interference, together with gain and loss saturation, affects the output intensities of PT-symmetric structures. A modified transfer matrix approach is employed, enabling a simultaneous examination of the impact of these nonlinear effects on the longitudinal field distribution. The resulting output intensity, reflectance, and transmittance characteristics are presented as functions of the input intensity for two cases in which the field distribution intensity is analyzed without and with taking into account the interference of counter-propagating waves, for different structure lengths, numbers of primitive cells, and saturation intensity levels. The results demonstrate that interference between counter-propagating waves significantly alters the output intensity, reflectance, and transmittance characteristics within the intermediate range of incident wave intensities, particularly for structures with small primitive cell sizes. Moreover, it modifies the bistability effect, causing the hysteresis loop to widen. Furthermore, in some configurations, this interference suppresses the unidirectional invisibility that would otherwise occur due to gain/loss saturation.

Keywords: parity-time symmetry; transfer matrix method; periodic lattice; nonlinear effects; spatial hole burning.

1. INTRODUCTION

Structures possessing PT (Parity–Time) symmetry have attracted significant interest since the late twentieth century [1]. In photonic systems, the design of PT-symmetric structures is fundamentally linked to the refractive indices of two layers forming a periodic lattice [2]. These layers are characterized by complex refractive indices of the form $n = n_{\mathrm{Re}} + in_{\mathrm{Im}}$, which satisfy the symmetry relation $n(x) = n^*(-x)$, where the asterisk denotes complex conjugation. This requirement can be considered independently for the real and imaginary components of the refractive index. In particular, the real part obeys $n_{\mathrm{Re}}(x) = n_{\mathrm{Re}}(-x)$, indicating spatial symmetry, whereas the imaginary part fulfills $n_{\mathrm{Im}}(x) = -n_{\mathrm{Im}}(-x)$, implying antisymmetry. The latter condition can be realized by combining two optically active materials, one providing gain ($n_{\mathrm{Im}} < 0$) and the other exhibiting loss ($n_{\mathrm{Im}} > 0$).

PT-symmetric structures have attracted considerable attention due to their distinctive physical phenomena, such as beam refraction [3], nonreciprocal light propagation [3], unidirectional invisibility [4], and coherent perfect absorption [5]. These systems have been investigated in various implementations, including photonic crystals [6], coupled PT-symmetric lattices [7], optical waveguide networks [8, 9], gain-assisted laser media [10, 11], and PT-symmetric magnetic metamaterial realized as coupled split-ring resonator arrays [12]. At the same time, the role of gain and loss saturation in PT-symmetric systems has been actively studied, for example, in the time domain [13], in Bragg gratings [14], in Fabry–Pérot lasers [15], in anti-PT symmetric structures [16], and together with the influence of the Kerr effect [17].

The interference of two counter-propagating waves produces a spatial intensity pattern (a standing wave). If the medium parameters depend nonlinearly on the optical intensity, such as through gain saturation or saturable absorption, the standing-wave intensity distribution induces a periodic modulation of the local gain or loss. This phenomenon is known as spatial hole burning (SHB) [18]. Such an effect in lasers leads to an uneven gain profile, which supplies energy to multiple modes, promotes competition among them, and results in unstable and irregular lasing behavior [19]. Spatial hole burning is also observed in DFB lasers [20]. In PT-symmetry lasers in the broken-phase regime, it is possible to efficiently eliminate spatial hole burning, thereby providing stable single-mode operation [21].

In this work, a theoretical investigation of how counter-propagating wave interference, together with gain and loss saturation, affects the output intensities of PT-symmetric non-laser structures is conducted for the first time. Multilayer PT-symmetric structures are analyzed using a modified transfer matrix method [13] that includes gain and loss saturation and considers incident waves of a specified intensity [15]. The model also takes into account the longitudinal variation in the field distribution across subsequent layers. Such an approach offers a straightforward way to evaluate how interference between

*e-mail: agnieszka.wyszynska@pw.edu.pl

Manuscript submitted 2026-07-02, revised 2026-08-26, initially accepted for publication 2026-08-26, published in November 2026.

© 2026 The Author(s). This is an open access article under the CC BY license (http://creativecommons.org/licenses/by/4.0/)

counter-propagating waves simultaneously influences the output intensities, reflectances, and transmittances of the structure. Moreover, a simplified optical method is used in the analysis, eliminating the need for computationally intensive techniques such as Transmission Line Modeling (TLM) [13].

The paper begins with a description of the procedure used to determine the refractive indices of PT-symmetric structures. Linear structural parameters adopted from previous studies [16] are used as the starting point. The effects of varying the number of primitive cells and gain/loss saturation parameters on multilayer PT structures are subsequently investigated. The results indicate nonlinear and bistable characteristics of the structure.

The theoretical formulation of the PT structure is presented in the next section, followed by Section 3, which illustrates the dependence of the output intensity, reflectances, and transmittances on the input intensity for different structural and saturation parameters. Section 4 summarizes the key findings.

2. THEORY

The PT-symmetric periodic structure analyzed here, shown in Fig. 1, is composed of alternating layers characterized by different complex refractive indices and described using a modified transfer matrix approach [13, 15, 16]. The gain layer is assigned a refractive index n_1, whereas the loss layer is defined by n_2. The surrounding medium is characterized by a refractive index n_0. As illustrated in Fig. 1, two configurations are considered: in the first (*setup 1*, Fig. 1a), the incident wave first encounters the gain layer, while in the second (*setup 2*, Fig. 1b), it initially interacts with the loss layer.

The following relations define the refractive indices:

$$n_1 = n_{\mathrm{Re}} - i\frac{n_{\mathrm{Im}}}{1+I_1/I_{s1}}, \quad n_2 = n_{\mathrm{Re}} + i\frac{n_{\mathrm{Im}}}{1+I_2/I_{s2}}, \tag{1}$$

where, for both layers, n_{Re} denotes the real part and n_{Im} represents the unsaturated imaginary part of the refractive indices, I_1 and I_2 are the electromagnetic wave intensities in the gain and loss layers, respectively. I_{s1} and I_{s2} are the corresponding saturation intensities of these layers.

The PT-symmetric structure under study consists of primitive cells, each composed of two layers of equal thickness, denoted w_a (for the gain layer) and w_b (for the loss layer). The total thickness of a single cell is $\Lambda = w_a + w_b$. The overall length of the structure is defined by the number of primitive cells N and the cell size Λ, giving $L = N\Lambda$.

The electric field distributions in the gain layer, $E_{1n}(x)$, and in the loss layer, $E_{2n}(x)$, can be represented as superpositions of two plane waves propagating in opposite directions along the X-axis (Fig. 1). As shown in [22], the complex amplitudes of these waves within the n-th cell are given by:

$$E_{1n}(x) = a_n \exp(ik_0 n_1 x) + b_n \exp(-ik_0 n_1 x), \tag{2a}$$

$$E_{2n}(x) = c_n \exp(ik_0 n_2 x) + d_n \exp(-ik_0 n_2 x), \tag{2b}$$

where a_n and b_n denote the complex amplitudes of the forward- and backward-propagating waves in the gain layer, while c_n and d_n correspond to those in the loss layer. The parameter k_0 represents the free-space wave number. The electromagnetic wave intensities I_1 and I_2 are related to the electric field distributions in the gain and loss layers of the primitive cells, respectively. Two cases are considered for I_1 and I_2: one in which the field distribution intensity is analyzed without and with taking into account the interference of counter-propagating waves and one in which this interference is included. The first case is designated $\eta = 0$, while the second is $\eta = 1$, similar to [20]. The corresponding intensities I_1 and I_2 are defined as follows:

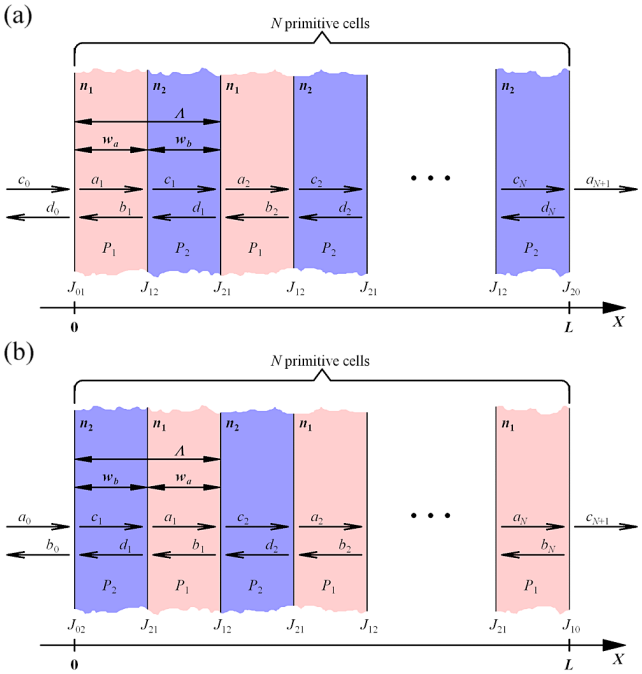


Fig. 1. PT-symmetric structures under consideration, with the junction (J) and propagation (P) matrices indicated [16]. (a) *setup 1* – the wave is incident on the gain layer; (b) *setup 2* – the wave is incident on the loss layer

$$\eta = 0 \quad \begin{cases} I_1 = |E_{1n}(x)|^2 = |a_n|^2 + |b_n|^2, \\ I_2 = |E_{2n}(x)|^2 = |c_n|^2 + |d_n|^2, \end{cases} \tag{3a}$$

$$\eta = 1 \quad \begin{cases} I_1 = |E_{1n}(x)|^2 = |a_n|^2 + |b_n|^2 \\ \qquad + a_n b_n^* \exp(ik_0 n_1 x) \\ \qquad + a_n^* b_n \exp(-ik_0 n_1 x), \\ I_2 = |E_{2n}(x)|^2 = |c_n|^2 + |d_n|^2 \\ \qquad + c_n d_n^* \exp(ik_0 n_2 x) \\ \qquad + c_n^* d_n \exp(-ik_0 n_2 x). \end{cases} \tag{3b}$$

The wave intensity depends on the layer first encountered (*setup 1* or *setup 2*). The input intensities $I_{\mathrm{in}}^{(1)}$ and $I_{\mathrm{in}}^{(2)}$, the reflected intensities $I_{\mathrm{ref}}^{(1)}$ and $I_{\mathrm{ref}}^{(2)}$, and the output intensities $I_{\mathrm{out}}^{(1)}$ and $I_{\mathrm{out}}^{(2)}$ for *setup 1* and *setup 2*, respectively, are defined as follows:

$$I_{\mathrm{in}}^{(1)} = |c_0|^2, \quad I_{\mathrm{ref}}^{(1)} = |d_0|^2, \quad I_{\mathrm{out}}^{(1)} = |a_{N+1}|^2, \tag{4a}$$

$$I_{\text{in}}^{(2)} = |a_0|^2, \quad I_{\text{ref}}^{(2)} = |b_0|^2, \quad I_{\text{out}}^{(2)} = |c_{N+1}|^2. \tag{4b}$$

In general, the reflectances $R^{(1)}$, $R^{(2)}$ and transmittances $T^{(1)}$, $T^{(2)}$ of the PT structures are expressed in terms of the field amplitudes:

$$R^{(1)} = \frac{I_{\text{ref}}^{(1)}}{I_{\text{in}}^{(1)}} = \left|\frac{d_0}{c_0}\right|^2, \qquad R^{(2)} = \frac{I_{\text{ref}}^{(2)}}{I_{\text{in}}^{(2)}} = \left|\frac{b_0}{a_0}\right|^2, \tag{5a}$$

$$T^{(1)} = \frac{I_{\text{out}}^{(1)}}{I_{\text{in}}^{(1)}} = \left|\frac{a_{N+1}}{c_0}\right|^2, \qquad T^{(2)} = \frac{I_{\text{out}}^{(2)}}{I_{\text{in}}^{(2)}} = \left|\frac{c_{N+1}}{a_0}\right|^2. \tag{5b}$$

The above relations are true for both linear and nonlinear structures and will be denoted, respectively, $R_{\text{lin}}^{(\{1,2\})}$ and $T_{\text{lin}}^{(\{1,2\})}$ in the linear case and $R_{\text{non}}^{(\{1,2\})}$ and $T_{\text{non}}^{(\{1,2\})}$ in the nonlinear case.

During light propagation through the analyzed layer, gain and loss saturation effects lead to variations in the imaginary part of the refractive index. This continuous change is approximated by discretization, in which a stepwise function replaces the smooth spatial profile of the imaginary component. As a result, each layer of the PT-symmetric cell is divided into thin slices, as shown in Fig. 2, where the subscript n denotes the primitive cell and the superscript (i) indicates the position of a given slice within the layer.

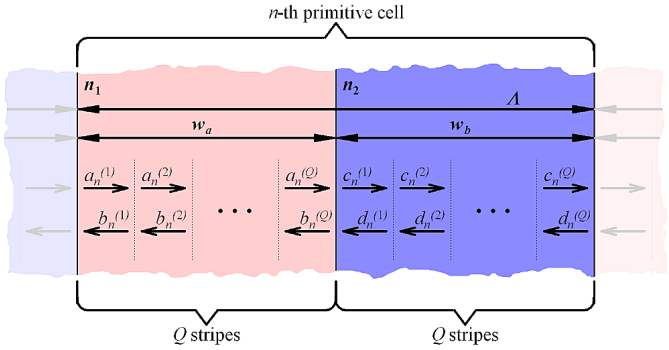


Fig. 2. Schematic representation of n-th PT cell divided into Q stripes [16]

The refractive indices in each stripe are given by:

$$n_1^{(i)} = n_{\text{Re}} - i\frac{n_{\text{Im}}}{1 + I_1^{(i)}/I_{s1}}, \quad n_2^{(i)} = n_{\text{Re}} + i\frac{n_{\text{Im}}}{1 + I_2^{(i)}/I_{s2}}, \tag{6}$$

where intensities $I_1^{(i)}$ and $I_2^{(i)}$ differ for the two setups, without and with the interference of counter-propagating waves. The following relations define them:

$$\eta = 0 \quad \begin{cases} I_1^{(i)} = \left|a_n^{(i)}\right|^2 + \left|b_n^{(i)}\right|^2, \\ I_2^{(i)} = \left|c_n^{(i)}\right|^2 + \left|d_n^{(i)}\right|^2, \end{cases} \tag{7a}$$

$$\eta = 1 \quad \begin{cases} I_1^{(i)} = \left|a_n^{(i)}\right|^2 + \left|b_n^{(i)}\right|^2 \\ \qquad + a_n^{(i)} b_n^{(i)*} \exp\left(ik_0 n_1^{(i)} x\right) \\ \qquad + a_n^{(i)*} b_n^{(i)} \exp\left(-ik_0 n_1^{(i)} x\right), \\ I_2^{(i)} = \left|c_n^{(i)}\right|^2 + \left|d_n^{(i)}\right|^2 \\ \qquad + c_n^{(i)} d_n^{(i)*} \exp\left(ik_0 n_2^{(i)} x\right) \\ \qquad + c_n^{(i)*} d_n^{(i)} \exp\left(-ik_0 n_2^{(i)} x\right). \end{cases} \tag{7b}$$

The accuracy of the calculations depends on the number of stripes Q per layer of the PT cell. This number must be sufficiently large to ensure that the refractive indices $n_1^{(i)}$ and $n_2^{(i)}$ remain approximately constant within each stripe, while the change in the refractive index between adjacent stripes is much smaller than the variation between the layers of the PT cell. The value of Q is determined by test calculations and chosen so that further increases have no effect on the results. The wave propagation through each stripe of the gain and loss layers, respectively, is described by the matrices $P_1^{(i)}$ and $P_2^{(i)}$, see equation (6) in Ref. [17]. The wave propagation through the boundary between layers with different refractive indices (i.e., the surrounding medium and the gain or loss layer, and the gain and loss layers of the primitive cell) is defined by the matrices J_{kl} ($k = 0, 1, 2$ and $l = 0, 1, 2$), see equation (7) in Ref. [17]. It is important to note that the equations involving the J matrix, which describe wave propagation across the interfaces between different media, are transcendental. Consequently, only approximate solutions can be obtained numerically using the so-called self-consistent method. In this approach, the equations are solved iteratively, with the resulting field amplitudes fed back into the J matrices until convergence is achieved. A detailed description of the J and P matrices can be found in the Appendices of Ref. [16].

The transfer matrices $M^{(1)}$ and $M^{(2)}$ connect the wave amplitudes on the two sides of the structures under study. For the two setups they are given by:

$$\begin{bmatrix} c_0 \\ d_0 \end{bmatrix} = M^{(1)} \begin{bmatrix} a_{N+1} \\ 0 \end{bmatrix}, \quad \begin{bmatrix} a_0 \\ b_0 \end{bmatrix} = M^{(2)} \begin{bmatrix} c_{N+1} \\ 0 \end{bmatrix}. \tag{8}$$

For a single primitive cell ($N = 1$), the matrices $M^{(1)}$ and $M^{(2)}$ are expressed as follows:

$$M^{(1)} = J_{01}\left(\prod_{i=1}^{Q} P_1^{(i)}\right) J_{12}\left(\prod_{i=1}^{Q} P_2^{(i)}\right) J_{20}, \tag{9a}$$

$$M^{(2)} = J_{02}\left(\prod_{i=1}^{Q} P_2^{(i)}\right) J_{21}\left(\prod_{i=1}^{Q} P_1^{(i)}\right) J_{10}. \tag{9b}$$

In the case of more than one cell ($N > 1$), the matrices take the following forms:

$$M^{(1)} = J_{01}\left[\prod_{i=1}^{N-1}\left(\prod_{i=1}^{Q} P_1^{(i)}\right)J_{12}\left(\prod_{i=1}^{Q} P_2^{(i)}\right)J_{21}\right] \cdot\left(\prod_{i=1}^{Q} P_1^{(i)}\right)J_{12}\left(\prod_{i=1}^{Q} P_2^{(i)}\right)J_{20}, \tag{10a}$$

$$M^{(2)} = J_{02}\left[\prod_{i=1}^{N-1}\left(\prod_{i=1}^{Q} P_2^{(i)}\right)J_{21}\left(\prod_{i=1}^{Q} P_1^{(i)}\right)J_{12}\right] \cdot\left(\prod_{i=1}^{Q} P_2^{(i)}\right)J_{21}\left(\prod_{i=1}^{Q} P_1^{(i)}\right)J_{10}. \tag{10b}$$

The output wave intensities, reflectances, and transmittances for both setups, without and with the interference of counter-propagating waves, are determined using equations (5)–(8), and (10), with the calculation procedure described in Appendix B of Ref. [16]. The following section presents the results of the numerical analysis of the investigated structure, highlighting the counter-propagating wave interference and gain/loss saturation on the output intensities. Specifically, $I_{\text{out}}^{(1)}$ corresponds to *setup 1*, where the wave exits the structure through the layer with refractive index n_2, and $I_{\text{out}}^{(2)}$ corresponds to *setup 2*, where the wave exits through the layer with refractive index n_1.

3. RESULTS AND DISCUSSION

The numerical analysis of the output wave intensity, reflectance, and transmittance of the PT structures requires specifying the refractive indices. The real part of the refractive index is set to a constant value of $n_{\text{Re}} = 3.165$, corresponding to the semiconductor material InP [23], while the imaginary part is set to $n_{\text{Im}} = 0.1$ [10], [14], [24]. The structures are assumed to be surrounded by air, with a refractive index of $n_0 = 1$. The operating wavelength is $\lambda = 1.55\mu m$, corresponding to the third telecommunications window.

Next, the size of a primitive cell (grating period Λ) and the number of such cells N are determined using a graph of reflectance $R_{\text{lin}}^{(\{1,2\})}$ and transmittance $T_{\text{lin}}^{(\{1,2\})}$ (calculated for the linear PT structure with all saturation effects omitted) as a function of the number of primitive cells N and the ratio Λ/λ of the grating period to the wavelength (see Fig. 3 of Ref. [16]). The graph presents two rows of maxima. Two cases from the first row were selected for analysis. The first corresponds to the smallest primitive cell size ($N = 25$ and $\Lambda/\lambda = 0.157849$). The second corresponds to the highest transmittance ($N = 21$ and $\Lambda/\lambda = 1.420474$). The analysis included structures characterized by the same ratio Λ/λ and a different number of primitive cells N.

Table 1 contains data obtained from calculations reported in Ref. [16]. For each row, the following parameters are listed: the number of primitive cells N, the ratio of the grating period to the operating wavelength Λ/λ, the overall length of the structure L, the linear reflectance $R_{\text{lin}}^{(1)}$ for *setup 1*, the linear reflectance $R_{\text{lin}}^{(2)}$ for *setup 2*, and the linear transmittances $T_{\text{lin}}^{(1)} = T_{\text{lin}}^{(2)}$ for both setups, which are equal to each other [14], [24]. The reflectances and transmittances are described by equation (5) in Ref. [16]. The PT structure parameters that provide maximal reflectance and transmittance (so-called peaks in the following text) are highlighted. It is worth noting that in these cases the reflectances for *setup 1* are significantly higher than those for *setup 2*. Data from Table 1 (particularly the number of primitive cells N and the ratio Λ/λ) serve as the starting point for the analysis of nonlinear PT structures presented in the following figures, whose numbers are indicated in the last column (Fig.) of Table 1.

The nonlinear analysis, incorporating counter-propagating wave interference and gain/loss saturation effects, is carried out for both investigated configurations of the nonlinear PT structures, using equations (5)–(10) from Section 2 of this work and the procedure described in Appendix B in Ref. [16]. To achieve sufficient computational accuracy, each layer of the structure is divided into $Q = 10$ segments (the value of Q is determined through test calculations).

Characteristics showing the output intensities $I_{\text{out}}^{(\{1,2\})}$, reflectances $R_{\text{non}}^{(\{1,2\})}$ and transmittances $T_{\text{non}}^{(\{1,2\})}$ as functions of the input wave intensity $I_{\text{in}}^{(\{1,2\})}$ were obtained for both setups (indicated by superscripts 1 and 2, respectively) and the structures listed in Table 1. The saturation intensity values chosen for this analysis are close to realistic values for InP-based structures [25]. The output intensity, reflectance, and transmittance characteristics are presented together because they constitute complementary characteristics of the same nonlinear response of the PT-symmetric structure. Their simultaneous analysis makes it possible to directly relate changes in the output intensity to the corresponding variations in reflectance and transmittance under identical physical conditions. This is particularly important when the interference of counter-propagating waves is taken into account, since the resulting modification of the longitudinal field distribution affects all three characteristics simultaneously. Additionally, the reflectance and transmittance levels equal to unity are marked with a black line on the appropriate charts for all the following characteristics (Figs. 3–6).

Table 1
Parameters of analyzed reflectance and transmittance maxima for the linear PT structures

N	Λ/λ	L (μm)	$R_{\text{lin}}^{(1)}$	$R_{\text{lin}}^{(2)}$	$T_{\text{lin}}^{(\{1,2\})}$	Fig.
21	0.157849	5.14	17.45	15.57	17.48	3 and 5
25	0.157849	6.12	7742.04	6892.06	7305.69	
29	0.157849	7.10	14.39	12.83	14.59	
17	1.420474	37.43	16.31	6.16	11.02	4 and 6
21	1.420474	46.24	19249.70	7205.17	11778.00	
25	1.420474	55.04	18.36	6.94	12.29	

Figure 3 shows the dependence of the output intensities, reflectances and transmittances on the input intensities for equal saturation intensities $I_{s1} = I_{s2} = 10^2$ W/cm^2 in both config-

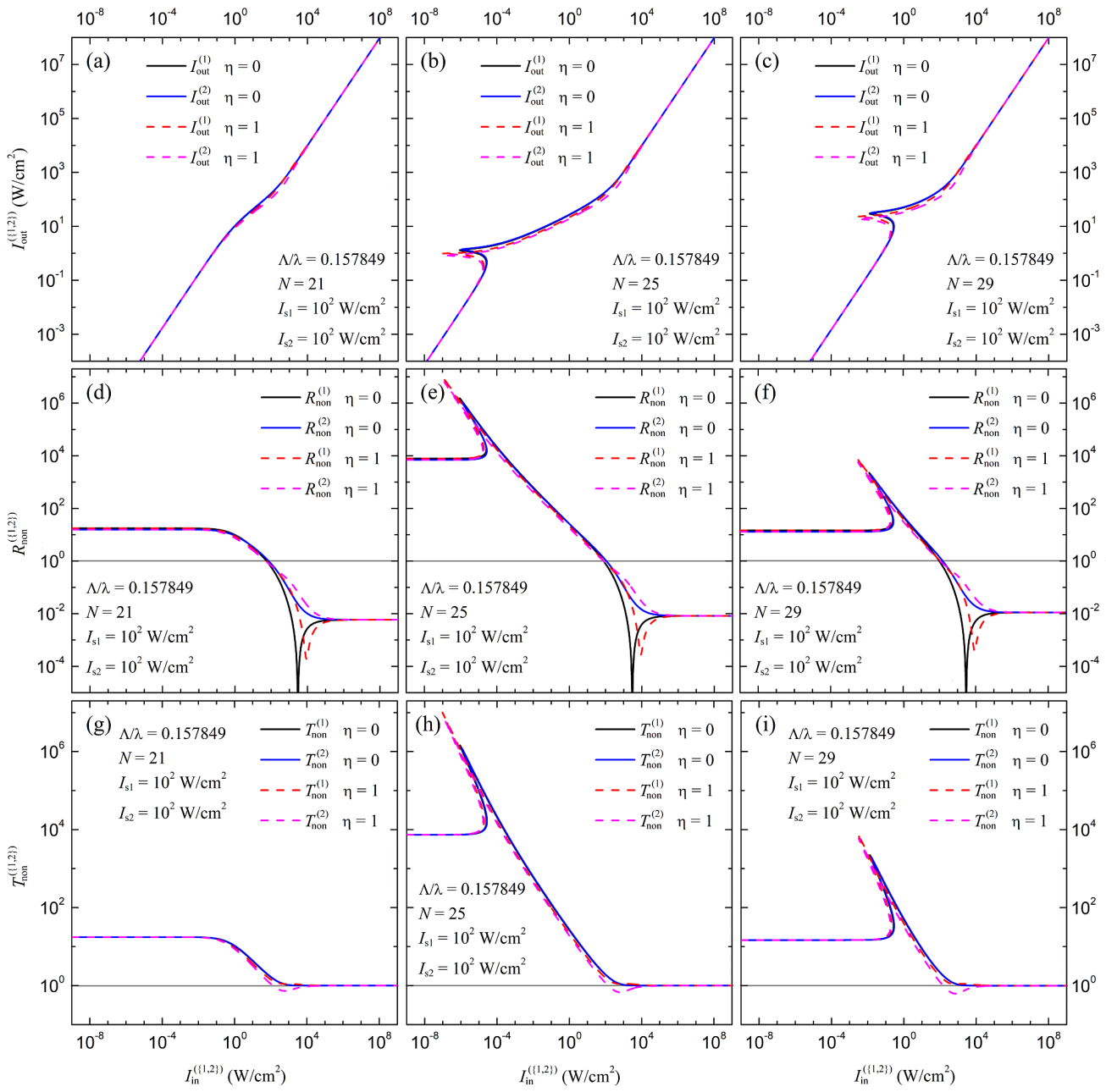


Fig. 3. Output intensities $I_{out}^{(\{1,2\})}$, reflectances $R_{non}^{(\{1,2\})}$ and transmittances $T_{non}^{(\{1,2\})}$ as a function of input intensity $I_{in}^{(\{1,2\})}$ shown for: both setups, ratio $\Lambda/\lambda = 0.157849$, saturation intensities $I_{s1} = I_{s2} = 10^2$ W/cm^2, without ($\eta = 0$) and with ($\eta = 1$) taking into account the interference of counter-propagating waves. The characteristics are plotted for different numbers N: (a), (d) and (g) $N = 21$; (b), (e) and (h) $N = 25$; (c), (f) and (i) $N = 29$

urations, for the ratio $\Lambda/\lambda = 0.157849$, without ($\eta = 0$) and with ($\eta = 1$) taking into account the interference of counter-propagating waves, and different primitive cell numbers N: (a), (d) and (g) $N = 21$; (b), (e) and (h) $N = 25$ (highlighted in Table 1); (c), (f) and (i) $N = 29$. It is worth noting that a change in the number of primitive cells N results in a change in the length of the entire structure L (see Table 1).

The presented characteristics behave similarly to those demonstrated in papers [16] and [17] for the case without taking into account wave interference ($\eta = 0$) and the case with such interference ($\eta = 1$), but only in the range of small and large values of the input intensities $I_{in}^{(\{1,2\})}$.

In the range of the medium values of $I_{in}^{(\{1,2\})}$, taking into account the interference of counter-propagating waves ($\eta = 1$) causes a slight reduction in the $I_{out}^{(\{1,2\})}$ value. The bistability effect, observed in the output wave intensities $I_{out}^{(\{1,2\})}$ characteristics, shifts toward smaller values of $I_{in}^{(\{1,2\})}$. It is worth noting that the hysteresis loops are wider when $\eta = 1$. The observed changes in $I_{out}^{(\{1,2\})}$ result from changes in the field distribution

due to the different length of the entire structure (see Fig. 9 in Ref. [26]). This field distribution determines the reflectance $R_{\text{non}}^{(\{1,2\})}$ and transmittance $T_{\text{non}}^{(\{1,2\})}$. Thus, the simultaneous presentation of these three characteristics facilitates the identification of the relationship between the nonlinear output response and the corresponding changes in reflection and transmission.

For input intensities above $I_{\text{in}}^{(\{1,2\})} = 10^2$ W/cm^2, in the case of *setup 1*, the reflectance $R_{\text{non}}^{(1)}$ shows a sharp decrease without ($\eta = 0$) and with ($\eta = 1$) taking into account the interference of counter-propagating waves. Moreover, for $\eta = 1$, its value is lower. This decrease is the so-called unidirectional invisibility effect. For *setup 2*, taking into account the interference of counter-propagating waves ($\eta = 1$) slightly increases the reflectance $R_{\text{non}}^{(2)}$ value compared with the case of $\eta = 0$.

In the case of the transmittances $T_{\text{non}}^{(\{1,2\})}$, for an input wave intensities of about $I_{\text{in}}^{(\{1,2\})} = 10^3$ W/cm^2, a local minimum is observed, occurring only for *setup 2* after taking into consideration the interference ($\eta = 1$). This minimum deepens as the number of primitive cells N increases.

Figure 4 demonstrates the dependence of the output intensities $I_{\text{out}}^{(\{1,2\})}$, reflectances $R_{\text{non}}^{(\{1,2\})}$ and transmittances $T_{\text{non}}^{(\{1,2\})}$

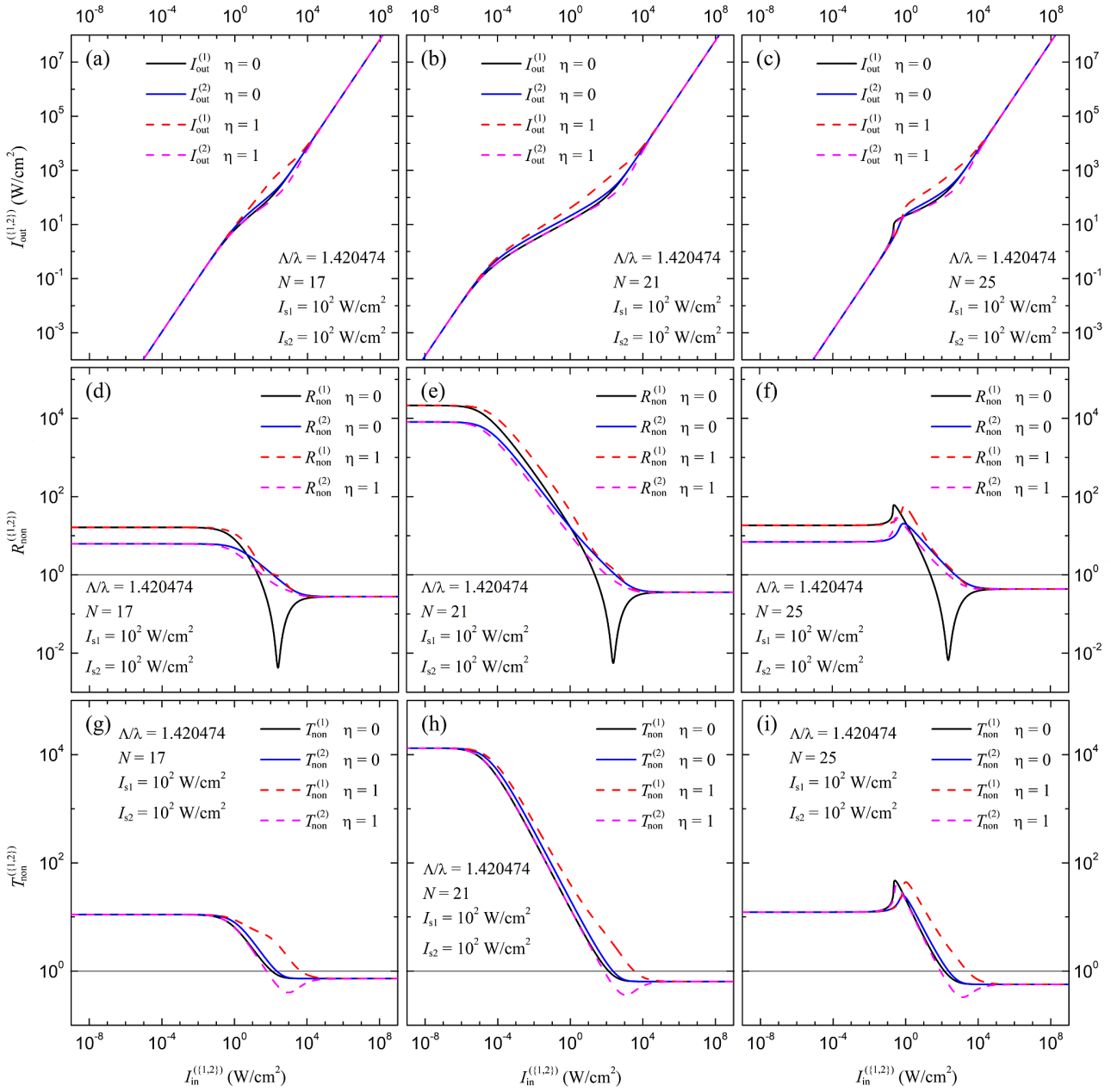


Fig. 4. Output intensities $I_{\text{out}}^{(\{1,2\})}$, reflectances $R_{\text{non}}^{(\{1,2\})}$ and transmittances $T_{\text{non}}^{(\{1,2\})}$ as a function of input intensity $I_{\text{in}}^{(\{1,2\})}$ shown for: both setups, ratio $\Lambda/\lambda = 1.420474$, saturation intensities $I_{s1} = I_{s2} = 10^2$ W/cm^2, without ($\eta = 0$) and with ($\eta = 1$) taking into account the interference of counter-propagating waves. The characteristics are plotted for different numbers N: (a), (d) and (g) $N = 17$; (b), (e) and (h) $N = 21$; (c), (f) and (i) $N = 25$

on the input intensities $I_{\text{in}}^{(\{1,2\})}$ for equal saturation intensities $I_{s1} = I_{s2} = 10^2$ W/cm^2 in both configurations, for the ratio $\Lambda/\lambda = 1.420474$, without ($\eta = 0$) and with ($\eta = 1$) taking into account the interference of counter-propagating waves, and different primitive cell numbers N: (a), (d) and (g) $N = 17$; (b), (e) and (h) $N = 21$ (highlighted in Table 1); (c), (f) and (i) $N = 25$. The overall length of the investigated structure L is much larger than that in the previous case presented in Fig. 3 (see Table 1), and increases with increasing number N.

As in Fig. 3, the influence of the interference of counter-propagating waves ($\eta = 1$) is observed for the medium range of the input intensities $I_{\text{in}}^{(\{1,2\})}$ only. Additionally, the differences in output intensities for both setups are greater than for $\eta = 0$, and the output intensity $I_{\text{out}}^{(1)}$ is higher than $I_{\text{out}}^{(2)}$.

The reflectances $R_{\text{non}}^{(\{1,2\})}$ characteristics are different from the corresponding characteristics in Fig. 3. In the medium range of the input intensities $I_{\text{in}}^{(\{1,2\})}$, where for the case without taking into account the interference of counter-propagating waves ($\eta = 0$), the unidirectional invisibility is observed, i.e., the reflectance $R_{\text{non}}^{(1)}$ tends to zero and the reflectance $R_{\text{non}}^{(2)}$ does not. When the interference of counter-propagating waves is taken into account ($\eta = 1$), the unidirectional invisibility effect

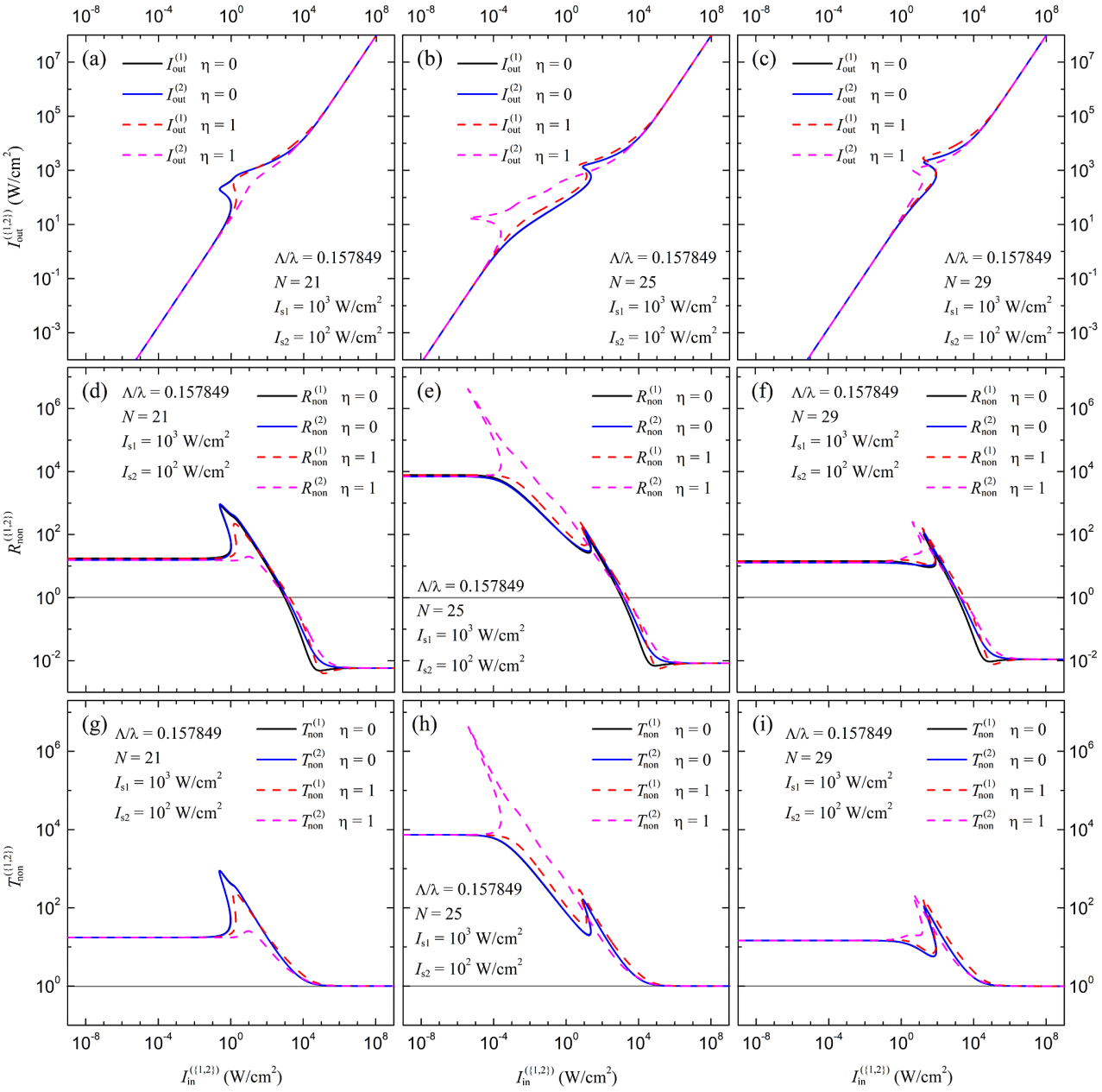


Fig. 5. Output intensities $I_{\text{out}}^{(\{1,2\})}$, reflectances $R_{\text{non}}^{(\{1,2\})}$ and transmittances $T_{\text{non}}^{(\{1,2\})}$ as a function of input intensity $I_{\text{in}}^{(\{1,2\})}$ shown for: both setups, ratio $\Lambda/\lambda = 0.157849$, saturation intensities $I_{s1} = 10^3$ W/cm^2 and $I_{s2} = 10^2$ W/cm^2, without ($\eta = 0$) and with ($\eta = 1$) taking into account the interference of counter-propagating waves. The characteristics are plotted for different numbers N and: (a), (d) and (g) $N = 21$; (b), (e) and (h) $N = 25$; (c), (f) and (i) $N = 29$

disappears and the reflectance $R_{\mathrm{non}}^{(1)}$ is greater than the reflectance $R_{\mathrm{non}}^{(2)}$. This behavior is caused by differences in the longitudinal field distribution between the two setups. This distribution is related to the size and number of the primitive cells.

Analogously to Fig. 3, in the medium range of the input intensities $I_{\mathrm{in}}^{(\{1,2\})}$, without considering interference from counter-propagating waves ($\eta = 0$), the transmittances $T_{\mathrm{non}}^{(\{1,2\})}$ almost overlap. Taking into account this interference ($\eta = 1$) results in the separation of the transmittance curves, and the transmittance $T_{\mathrm{non}}^{(1)}$ is greater than $T_{\mathrm{non}}^{(2)}$. Moreover, the transmittance $T_{\mathrm{non}}^{(2)}$ has noticeable minimum.

Figure 5 presents the dependence of the output intensities, reflectances and transmittances on the input intensities for different saturation intensities $I_{s1} = 10^3$ W/cm^2 and $I_{s2} = 10^2$ W/cm^2 in both configurations, for the ratio $\Lambda/\lambda = 0.157849$, without ($\eta = 0$) and with ($\eta = 1$) taking into account the interference of counter-propagating waves, and different primitive cell numbers N: (a), (d) and (g) $N = 21$; (b), (e) and (h) $N = 25$ (highlighted in Table 1); (c), (f) and (i) $N = 29$. Note that a variation in the number of primitive cells N leads to a corresponding change in the overall length of the structure L (see Table 1).

Introducing a difference in the saturation intensities of the gain and loss layers makes the influence of the interference on

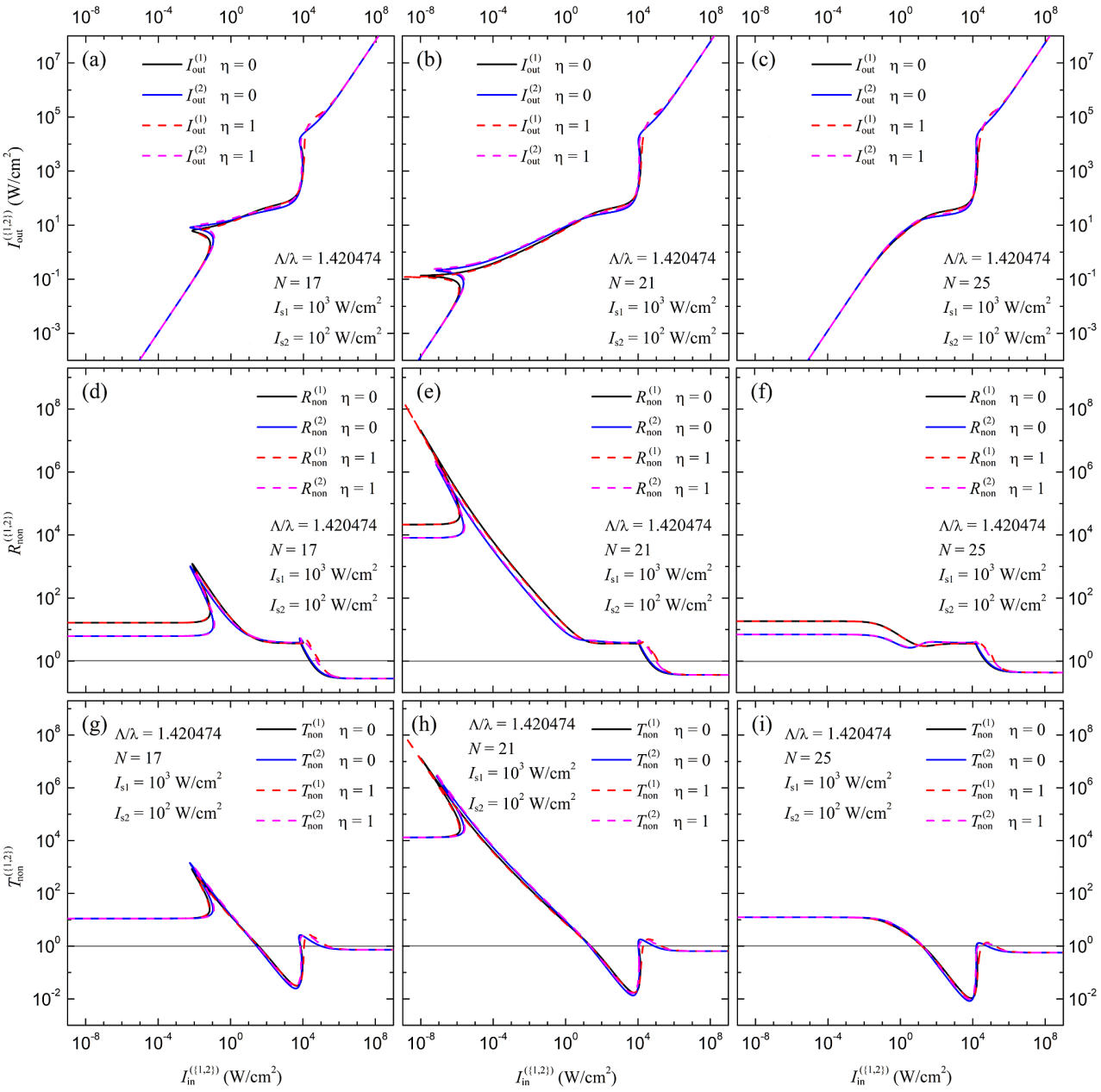


Fig. 6. Output intensities $I_{\mathrm{out}}^{(\{1,2\})}$, reflectances $R_{\mathrm{non}}^{(\{1,2\})}$ and transmittances $T_{\mathrm{non}}^{(\{1,2\})}$ as a function of input intensity $I_{\mathrm{in}}^{(\{1,2\})}$ shown for: both setups, ratio $\Lambda/\lambda = 1.420474$, saturation intensities $I_{s1} = 10^3$ W/cm^2 and $I_{s2} = 10^2$ W/cm^2, without ($\eta = 0$) and with ($\eta = 1$) taking into account the interference of counter-propagating waves. The characteristics are plotted for different numbers N: (a), (d) and (g) $N = 17$; (b), (e) and (h) $N = 21$; (c), (f) and (i) $N = 25$

the studied characteristics more visible. It is worth emphasizing that, in this case, the loss layer saturates more quickly, so the gain layer has a stronger effect on the propagating wave.

Similar to the previous characteristics, the influence of the interference of counter-propagating waves is visible only in the middle range of $I_{\text{in}}^{(\{1,2\})}$. For the primitive cell number $N = 21$ (a smaller value than for the peak of reflectance and transmittance highlighted in Table 1), the interference ($\eta = 1$) causes a decrease in the values of $I_{\text{out}}^{(\{1,2\})}$, $R_{\text{non}}^{(\{1,2\})}$ and $T_{\text{non}}^{(\{1,2\})}$. This decrease is stronger in *setup 2* (where the wave exits the PT structure through the gain layer), and the bistability effect disappears.

In the case of $N = 25$ primitive cells (at the peak of maximal reflectance and transmittance for the linear PT structure), taking into account the interference of counter-propagating waves ($\eta = 1$) results in greater changes of $I_{\text{out}}^{(\{1,2\})}$, $R_{\text{non}}^{(\{1,2\})}$ and $T_{\text{non}}^{(\{1,2\})}$ characteristics. For *setup 1*, the output intensities, reflectances, and transmittance characteristics almost overlap with those for ($\eta = 0$), respectively. For *setup 2*, considering interference ($\eta = 1$) shifts the bistability toward smaller input intensities $I_{\text{in}}^{(\{1,2\})}$. Furthermore, the new hysteresis loop is wider. Simultaneously, the $I_{\text{out}}^{(\{1,2\})}$, $R_{\text{non}}^{(\{1,2\})}$ and $T_{\text{non}}^{(\{1,2\})}$ values for $\eta = 1$ and *setup 2* are much larger than for $\eta = 0$ for both setups, respectively.

A further increase in the number of primitive cells to $N = 29$ (a larger number of cells than for the reflectance and transmittance peak) with interference taken into account ($\eta = 1$) causes a small increase in the output intensities $I_{\text{out}}^{(\{1,2\})}$, reflectances $R_{\text{non}}^{(\{1,2\})}$ and transmittances $T_{\text{non}}^{(\{1,2\})}$ above the corresponding values of $I_{\text{out}}^{(\{1,2\})}$, $R_{\text{non}}^{(\{1,2\})}$ and $T_{\text{non}}^{(\{1,2\})}$ for $\eta = 0$. However, despite the medium's larger volume, detuning from the peak ($N = 25$) reduces reflectances $R_{\text{non}}^{(\{1,2\})}$ and transmittances $T_{\text{non}}^{(\{1,2\})}$ for $\eta = 1$.

Figure 6 shows the dependence of the output intensities $I_{\text{out}}^{(\{1,2\})}$, reflectances $R_{\text{non}}^{(\{1,2\})}$ and transmittances $T_{\text{non}}^{(\{1,2\})}$ on the input intensities $I_{\text{in}}^{(\{1,2\})}$ for different saturation intensities $I_{s1} = 10^3$ W/cm^2 and $I_{s2} = 10^2$ W/cm^2 in both configurations, for the ratio $\Lambda/\lambda = 1.420474$, without ($\eta = 0$) and with ($\eta = 1$) taking into account the interference of counter-propagating waves, and different primitive cell numbers N: (a), (d) and (g) $N = 17$; (b), (e) and (h) $N = 21$ (highlighted in Table 1); (c), (f) and (i) $N = 25$. The total length of the PT structure L is much larger than for the previous case presented in Fig. 5 (see Table 1), and increases with increasing number N.

In general, for both setups, taking into account the interference of counter-propagating waves ($\eta = 1$) causes slight changes in the output intensities $I_{\text{out}}^{(\{1,2\})}$, reflectances $R_{\text{non}}^{(\{1,2\})}$ and transmittances $T_{\text{non}}^{(\{1,2\})}$ only for input intensities around $I_{\text{in}}^{(\{1,2\})} = 10^4$ W/cm^2 for all investigated numbers of primitive cells (i.e. $N = 17, 21, 25$).

In contrast to Fig. 4, introducing a difference in the saturation intensities of the gain and loss layers (I_{s1} and I_{s2}) causes the appearance of the bistability effect for the number of primitive cells equal to $N = 17$ and $N = 21$ in the range of medium and small values of the input intensities $I_{\text{in}}^{(\{1,2\})}$, respectively. Taking into account the interference of counter-propagating waves ($\eta = 1$) results in noticeable differences in the output intensities $I_{\text{out}}^{(\{1,2\})}$, reflectances $R_{\text{non}}^{(\{1,2\})}$ and transmittances $T_{\text{non}}^{(\{1,2\})}$ compared with the corresponding quantities for $\eta = 0$, but only for the number of primitive cells equal to $N = 21$ (at the peak of maximal reflectance and transmittance for the linear PT structure). The hysteresis loop widens, especially for the output intensities, reflectances, and transmittance values for *setup 1*. The simultaneous changes observed in the output intensity, reflectance, and transmittance are particularly relevant for the interpretation of the bistable response, since the position and width of the hysteresis loops are modified together with the corresponding reflection and transmission characteristics.

For primitive cell number $N = 25$ (a greater value than for the peak of reflectance and transmittance highlighted in Table 1), the output intensities $I_{\text{out}}^{(\{1,2\})}$, reflectances $R_{\text{non}}^{(\{1,2\})}$ and transmittances $T_{\text{non}}^{(\{1,2\})}$ characteristics overlap without ($\eta = 0$) and with ($\eta = 1$) taking into account the interference of counter-propagating waves for both setups.

4. CONCLUSIONS

This work presents the output intensities, reflectances, and transmittances of finite nonlinear PT-symmetric structures illuminated by plane waves of specified intensity, taking into account the interference of counter-propagating waves as well as different gain/loss saturation levels. Two configurations are considered: *setup 1*, in which the incident wave illuminates the gain layer with refractive index n_1, and *setup 2*, in which the wave illuminates the loss layer with refractive index n_2.

A modified transfer-matrix method is used for the nonlinear analysis. This approach requires a self-consistent procedure to determine the matrices that describe wave propagation across the interfaces between all layers in the PT structure. Importantly, the refractive indices of the layers are modulated by both interference between counter-propagating waves and gain/loss saturation, which, in turn, influence the longitudinal field distribution in subsequent layers.

The main conclusions from the analyses conducted are summarized below. The influence of counter-propagating wave interference on the characteristics depends strongly on the size of the primitive cells and the number of cells forming the PT structure. Moreover, it modifies the bistability effect, which depends on the gain/loss saturation intensities. When the saturation intensities of the gain and loss layers are identical, the interference effect is stronger in the PT structure with large primitive cell sizes (the structure exhibits maximal reflectance and transmittance). In this case, the output intensity and transmittance are higher for *setup 1* than in the case without taking into account the interference effect. Additionally, the unidirectional invisibility effect disappears from the reflectance characteristics.

When the saturation intensity of the gain layer is greater than that of the loss layer, the interference effect is stronger in the PT structure with small primitive cell sizes, especially for *setup 2* and for the structure corresponding to the maximal reflectance and transmittance in the linear PT structure. In this case, bistability occurs at lower input intensities. The proposed model is a useful tool for simulating PT structures and can be applied to a wide range of materials. The obtained results may be relevant

to the development of nonlinear PT-symmetric photonic devices for optical switching, tunable light transmission, and optical signal processing. In particular, the demonstrated sensitivity of the output characteristics and bistable response to the interference of counter-propagating waves, the number of primitive cells, and the gain/loss saturation levels may be useful for designing tunable all-optical functionalities.

ACKNOWLEDGEMENTS

The authors would like to express their gratitude to Ms Urszula Wyszyńska for reviewing the manuscript for linguistic accuracy.

REFERENCES

[1] C.M. Bender and S. Boettcher, "Real Spectra in Non-Hermitian Hamiltonians Having PT Symmetry," *Phys. Rev. Lett.*, vol. 80, no. 24, pp. 5243–5246, 1998, doi: 10.1103/PhysRevLett.80.5243.

[2] R. El-Ganainy, K.G. Makris, D.N. Christodoulides, and Z.H. Musslimani, "Theory of coupled optical PT-symmetric structures," *Opt. Lett.*, vol. 32, no. 17, pp. 2632–2634, 2007, doi: 10.1364/OL.32.002632.

[3] K.G. Makris, R. El-Ganainy, D.N. Christodoulides, and Z.H. Musslimani, "Beam Dynamics in PT Symmetric Optical Lattices," *Phys. Rev. Lett.*, vol. 100, no. 10, p. 103904, 2008, doi: 10.1103/PhysRevLett.100.103904.

[4] Z. Lin, H. Ramezani, T. Eichelkraut, T. Kottos, H. Cao, and D.N. Christodoulides, "Unidirectional Invisibility Induced by PT-Symmetric Periodic Structures," *Phys. Rev. Lett.*, vol. 106, no. 21, p. 213901, 2011, doi: 10.1103/PhysRevLett.106.213901.

[5] Y. Sun, W. Tan, H.-q. Li, J. Li, and H. Chen, "Experimental Demonstration of a Coherent Perfect Absorber with PT Phase Transition," *Phys. Rev. Lett.*, vol. 112, no. 14, p. 143903, 2014, doi: 10.1103/PhysRevLett.112.143903.

[6] S. Longhi, "Bloch Oscillations in Complex Crystals with PT Symmetry," *Phys. Rev. Lett.*, vol. 103, no. 12, p. 123601, 2009, doi: 10.1103/PhysRevLett.103.123601.

[7] M.-A. Miri, A. Regensburger, U. Peschel, and D.N. Christodoulides, "Optical mesh lattices with PT symmetry," *Phys. Rev. A*, vol. 86, no. 2, p. 023807, 2012, doi: 10.1103/PhysRevA.86.023807.

[8] S.V. Suchkov, A.A. Sukhorukov, J. Huang, S.V. Dmitriev, C. Lee, and Y.S. Kivshar, "Nonlinear switching and solitons in PT-symmetric photonic systems," *Laser Photonics Rev.*, vol. 10, no. 2, pp. 177–213, 2016, doi: 10.1002/lpor.201500227.

[9] J. Wu and X. Yang, "Ultrastrong extraordinary transmission and reflection in PT-symmetric Thue-Morse optical waveguide networks," *Opt. Express*, vol. 25, no. 22, pp. 27 724–27 735, 2017, doi: 10.1364/OE.25.027724.

[10] L. Feng, Z.J. Wong, R.-M. Ma, Y. Wang, and X. Zhang, "Single-mode laser by parity-time symmetry breaking," *Science*, vol. 346, no. 6212, pp. 972–975, 2014, doi: 10.1126/science.1258479.

[11] H. Benisty, V.B. d. l. Perrière, A. Ramdane, and A. Lupu, "Parity-time symmetric gratings in 1550 nm distributed-feedback laser diodes: insight on device design rules," *J. Opt. Soc. Am. B*, vol. 38, no. 9, pp. C168–C174, 2021, doi: 10.1364/JOSAB.428638.

[12] M. I. Molina, "Bounded dynamics in finite PT-symmetric magnetic metamaterials," *Phys. Rev. E*, vol. 89, no. 3, p. 033201, 2014, doi: 10.1103/PhysRevE.89.033201.

[13] S. Phang, "Theory and Numerical Modelling of Parity-Time Symmetric Structures for Photonics," 2016. [Online]. Available: http://eprints.nottingham.ac.uk/32596/

[14] P. Witoński, A. Mossakowska-Wyszyńska, and P. Szczepański, "Effect of Nonlinear Loss and Gain in Multilayer PT-Symmetric Bragg Grating," *IEEE J. Quant. Electron.*, vol. 53, no. 6, p. 8063405, 2017, doi: 10.1109/JQE.2017.2761380.

[15] A. Mossakowska-Wyszyńska, P. Witoński, and P. Szczepański, "Nonlinear operation of an FP laser with PT symmetry active medium," *Opt. Express*, vol. 31, no. 5, pp. 8518–8534, 2023, doi: 10.1364/OE.479222.

[16] A. Mossakowska-Wyszyńska, P. Witoński, and P. Szczepański, "Analysis of nonlinear response of anti-parity-time symmetric structure," *Opto-Electron. Rev.*, vol. 33, no. 2, p. e154198, 2025, doi: 10.24425/opelre.2025.154198.

[17] P. Witoński, A. Mossakowska-Wyszyńska, and P. Szczepański, "Influence of the Kerr effect on the properties of nonlinear PT-symmetric structures," *Opt. Express*, vol. 33, no. 26, pp. 54 680–54 694, 2025, doi: 10.1364/OE.578645.

[18] G.P. Agrawal, "Intracavity resonant degenerate four-wave mixing: bistability in phase conjugation," *J. Opt. Soc. Am.*, vol. 73, no. 5, pp. 654–660, 1983, doi: 10.1364/JOSA.73.000654.

[19] Z. Zhang, P. Miao, J. Sun, S. Longhi, N.M. Litchinitser, and L. Feng, "Elimination of Spatial Hole Burning in Microlasers for Stability and Efficiency Enhancement," *ACS Photonics*, vol. 5, no. 8, pp. 3016–3022, 2018, doi: 10.1021/acsphotonics.8b00800.

[20] A. Mossakowska, P. Szczepański, and W. Woliński, "Influence of spatial hole burning effects on relaxation oscillations in waveguide distributed feedback Nd3+:YAG lasers," *Opt. Commun.*, vol. 100, no. 1, pp. 153–158, 1993, doi: 10.1016/0030-4018(93)90572-M.

[21] J.-F. Bisson and Y.C. Nonguierma, "Single-mode lasers using parity-time-symmetric polarization eigenstates," *Phys. Rev. A*, vol. 102, no. 4, p. 043522, 2020, doi: 10.1103/PhysRevA.102.043522.

[22] P. Witoński, A. Mossakowska-Wyszyńska, and P. Szczepański, "Gain Properties of the Single Cell of a One-Dimensional Photonic Crystal with PT Symmetry," *Crystals*, vol. 13, no. 2, p. 258, 2023, doi: 10.3390/cryst13020258.

[23] G.D. Pettit and W.J. Turner, "Refractive Index of InP," *J. Appl. Phys.*, vol. 36, no. 6, p. 2081, 1965, doi: 10.1063/1.1714410.

[24] O.V. Shramkova and G.P. Tsironis, "Resonant Combinatorial Frequency Generation Induced by a PT-Symmetric Periodic Layered Stack," *IEEE J. Sel. Top. Quantum Electron.*, vol. 22, no. 5, pp. 82–88, 2016, doi: 10.1109/JSTQE.2015.2505139.

[25] H. Haug and L. Banyai, Eds., *Optical Switching in Low-Dimensional Systems*, ser. Nato Science Series B: Springer US, 1989.

[26] A. Mossakowska-Wyszyńska, P. Witoński, and P. Szczepański, "Operation of Fabry-Perot laser with nonlinear PT-symmetric mirror," *Bull. Pol. Acad. Sci. Tech. Sci.*, vol. 69, no. 6, p. e139202, 2021, doi: 10.24425/bpasts.2021.139202.